Applied Catalysis B: Environmental 136–137 (2013) 193–201

Contents lists available at SciVerse ScienceDirect

Applied Catalysis B: Environmental

journal homepage: www.elsevier.com/locate/apcatb

Design and synthesis of hydrophobic and stable mesoporous polymeric solid acid with ultra strong acid strength and excellent catalytic activities for biomass transformation

Fujian Liu[a,c,*], Anmin Zheng[b,**], Iman Noshadi[d], Feng-Shou Xiao[c]

[a] Zhejiang Key Laboratory of Alternative Technologies for Fine Chemicals Process, Shaoxing University, 312000, China
[b] Wuhan Center for Magnetic Resonance, State Key Laboratory of Magnetic Resonance and Atomic and Molecular Physics, Wuhan Institute of Physics and Mathematics, Chinese Academy of Sciences, Wuhan 430071, China
[c] Key Lab of Applied Chemistry of Zhejiang Province, Department of Chemistry, Zhejiang University (XiXi Campus), Hangzhou 310028, China
[d] Institute of Materials Science, University of Connecticut, Storrs, CT 06269, United States

ARTICLE INFO

Article history:
Received 12 October 2012
Received in revised form 23 January 2013
Accepted 29 January 2013
Available online 14 February 2013

Keywords:
Solid strong acid
Mesoporous polymers
Hydrophobicity
Wettability
Biomass transformation

ABSTRACT

Novel and efficient mesoporous polydivinylbenzene (PDVB) based solid strong acid (PDVB-SO_3H-SO_2CF_3) has been successfully prepared by grafting of strong electron withdrawing group of —SO_2CF_3 onto the network of performed mesoporous solid acid of PDVB-SO_3H, which could be synthesized from sulfonation of superhydrophobic mesoporous PDVB or copolymerization of DVB with sodium *p*-styrene sulfonate. Characterizations of N_2 sorption isotherms, TG curves and contact angle tests show that PDVB-SO_3H-SO_2CF_3 has large Brunauer–Emmett–Teller (BET) surface area, superior thermal stability, good hydrophobicity and oleophilicity. Solid ^{31}P NMR spectra and NH_3–TPD curves show that the Brønsted acidic site in PDVB-SO_3H-SO_2CF_3 has been significantly enhanced and rather homogeneously distributed when compared with that of PDVB-SO_3H. Catalytic tests show that PDVB-SO_3H-SO_2CF_3 exhibits excellent catalytic activities and good recyclability in biomass transformation toward transesterification to biodiesel and depolymerization of crystalline cellulose to sugars when compared with those of PDVB-SO_3H, solid strong acids of SO_4/ZrO_2 and Nafion NR50. The excellent catalytic activity and good recyclability of PDVB-SO_3H-SO_2CF_3 result from its unique characters such as large surface area, ultra strong acid strength, adjustable hydrophobic–oleophilic and stable network.

1. Introduction

During the last two decades, acid catalysis have received considerable attention because of their wide applications in the areas of oil refining, biomass transformation, green chemical processes and fine chemical industry [1–26]. Among various acid catalysts, the fluorine containing acids such as CF_3SO_3H, HF-SbF_5 show very important applications because of their ultra strong acid strength when compared with conventional mineral acids such as H_2SO_4 and HCl [27–30], which results from the presence of strong electron withdrawing groups in these acids. The unique strong acid strength results in their extra-ordinary catalytic activities in various reactions such as alkylation, isomerization, oligocondensation reactions of alkanes, Friedel–Crafts, polymerization, Koch carbonylation, cracking and biomass transformation [27,31]. However, homogeneous superacids are usually highly toxic, environmentally hazardous, and cannot be easily recovered from the products mixture, which largely constrain their wide applications in industry [31].

The successfully preparation of solid strong acids has basically overcome the problems caused by homogeneous strong acids because of their characters including reductive corrosion, environmentally friendly, superior catalytic activities, good catalytic selectivity and recyclability. Typically solid strong acids such as sulfated metal oxides and heteropolyacids have been widely used in various acid-catalyzed reactions including esterifications, isomerization, transesterifications and Friedel–Crafts [32–37], which are more active than the solid acids with relatively weak acid strength [32–36]. However, the existed drawbacks such as low BET surface areas, partial deactivation of the active sites by the water resulted from the hydrophilic frameworks largely decrease their catalytic activities and lives, which was attributed to the water usually act as a typical byproduct in many acid-catalyzed reactions, further resulting in the opposite reactions and the leaching of active sites [8,9,38–42].

* Corresponding author at: Zhejiang Key Laboratory of Alternative Technologies for Fine Chemicals Process, Shaoxing University, 312000, China.
Tel.: +86 575 88345682; fax: +86 575 88345682.
** Corresponding author.
E-mail addresses: liufujian1982@yahoo.cn (F. Liu), zhenganm@wipm.ac.cn (A. Zheng).

0926-3373/$ – see front matter © 2013 Elsevier B.V. All rights reserved.
http://dx.doi.org/10.1016/j.apcatb.2013.01.063

The presence of Nafion type of acidic resin offers great opportunities for the synthesis of solid strong acids ($pK_a \approx -12$) with hydrophobic polymer network, which was thought to be one of the strongest solid acids [43–45], giving excellent thermal stability and good catalytic activities [46–48]. However, its very low concentration of acidic site and poor porosity largely constrain it used as efficient solid acid in various acid-catalyzed reactions [43,45].

Therefore, synthesis of solid acids with enhanced acid strength, adjustable hydrophobicity and abundant nanoporosity are the crucial problems faced to the scientists working on heterogeneous acid catalysis. However, it is still challenging to synthesize solid acids with large BET surface areas, ultra strong acid strength, adjustable hydrophobic networks, and high contents of acid sites up to now, which would be very important for their wide applications [8,9,35,39–42,49–54].

We report here the successfully preparation of mesoporous polymeric solid acid (PDVB-SO_3H-SO_2CF_3) with large BET surface areas, good hydrophobicity and oleophilicity, superior thermal stability, and ultra strong acid strength through grafting of strong electron withdrawing group of SO_2CF_3 onto the network of mesoporous solid acid of PDVB-SO_3H, which could be synthesized from sulfonation of superhydrophobic mesoporous PDVB or copolymerization of DVB with sodium *p*-styrene sulfonate. Interestingly, the resulted PDVB-SO_3H-SO_2CF_3 showed much better catalytic activities and recyclability in biomass transformation toward depolymerization of crystalline cellulose to sugars and transesterification to biodiesel, Peckmann reaction of resorcinol with ethyl acetoacetate (PRE) and hydration of propylene oxide with water (HPW) than those of PDVB-SO_3H, Amberlyst 15, sulfonic groups functional mesoporous silica (SBA-15-SO_3H), and solid strong acids of SO_4/ZrO_2 and Nafion NR50. The successfully preparation of PDVB-SO_3H-SO_2CF_3 will open a new way for preparation of efficient and long lived mesoporous polymeric solid strong acid for catalyzing transformation of biomass into biofuels with large scale in industry.

2. Experimental

2.1. Chemicals and regents

All reagents were of analytical grade and used as purchased without further purification. Amberlyst 15, 3-mercaptopropyltrimethoxysilane (3-MPTS), crystalline cellulose of Avicel, tripalmitin, nonionic block copolymer surfactant of poly(ethyleneoxide)–poly(propyleneoxide)–poly(ethyleneoxide) block copolymer (Pluronic 123, molecular weight of about 5800), sodium *p*-styrene sulfonate and trifluoromethanesulfonate were purchased from Sigma–Aldrich Company, Ltd. (USA). DVB, azobisisobutyronitrile (AIBN), tetrahydrofuran (THF), tetraethyl orthosilicate (TEOS), chlorosulfonic acid, dichlormethane, resorcinol, ethyl acetoacetate, methanol, propylene oxide, and dodecane were obtained from Tianjin Guangfu Chemical Reagent. H-form of Beta zeolite and ultrastable Y zeolite (USY) were supplied by Sinopec Catalyst Co.

2.2. Synthesis of samples

2.2.1. Synthesis of superhydrophobic mesoporous PDVB

Superhydrophobic mesoporous PDVB was synthesized by polymerization of DVB under solvothermal condition with starting system of DVB/AIBN/THF/H_2O at molar ratio of 1/0.02/16.1/7.23. As a typical run, 2.0 g of DVB was added into a solution containing of 0.05 g of AIBN and 20 mL of THF, followed by addition of 2 mL of H_2O. After stirring at room temperature for 3 h, the mixture was transferred into an autoclave and treated at 100 °C for 1 day. After evaporation of the solvents at room temperature, the mesoporous PDVB with monolithic morphology and opened mesopores was obtained.

2.2.2. Synthesis of PDVB-SO_3H

PDVB-SO_3H was synthesized by stirring of PDVB in the mixture of chlorosulfonic acid and CH_2Cl_2. As a typical run, 1.5 g of PDVB was outgassed at 100 °C in a three-necked round flask for 12 h under flowing nitrogen. Then, a mixture containing 40 mL of CH_2Cl_2 and 20 mL of chlorosulfonic acid was quickly added into the flask below 10 °C. After stirring for 24 h under nitrogen atmosphere, the product was obtained from filtering, washing with large amount of water for removing of residual sulfuric acid, stirring in dioxane, and drying at 80 °C under vacuum.

In the meanwhile, PDVB-SO_3H could also be synthesized from copolymerization of DVB with sodium *p*-styrene sulfonate under solvothermal condition, and the content of sulfonic group could be adjusted by changing of the molar ratio of DVB and sodium *p*-styrene sulfonate. As a typical run, 2.0 g of DVB was added into a solution containing 0.05 g of AIBN and 28 mL of THF, followed by addition of 2.5 mL of H_2O, then 0.64 g of sodium *p*-styrene sulfonate was also introduced. After stirring at room temperature for 3 h to form a homogeneous solution, the mixture was solvothermally treated at 100 °C for 24 h. After evaporation of the solvents at room temperature, the PDVB-SO_3Na sample with monolithic morphology was obtained. To get a PDVB-SO_3H sample, the PDVB-SO_3Na sample was further ion-exchanged using 1 M sulfuric acid. As a typical run, 0.5 g of PDVB-SO_3Na was dispersed into 50 mL of 1 M sulfuric acid. After stirring for 24 h at room temperature, the sample was washed with large amount of water until the filtrate was neutral, drying at 80 °C, PDVB-SO_3H was obtained.

2.2.3. Synthesis of solid strong acid of PDVB-SO_3H-SO_2CF_3

Strong solid acid of PDVB-SO_3H-SO_2CF_3 was synthesized from the treatment of PDVB-SO_3H by using of HSO_3CF_3, which results in grafting of strong electron withdrawing group of —SO_2CF_3 onto the network of PDVB-SO_3H. As a typical run, 1.5 g of PDVB-SO_3H was added into a flask containing 50 mL of toluene, followed by addition of 10 mL of HSO_3CF_3, then the reaction temperature was rapidly increased to 100 °C, after stirring for another 24 h, PDVB-SO_3H-SO_2CF_3 was obtained from filtration, washing with large amount of CH_2Cl_2, and drying at 80 °C under vacuum.

For comparison, SBA-15-SO_3H with molar ratios of S/Si at 0.1 and SO_4/ZrO_2 were synthesized according to the literature [38,55].

2.3. Characterizations

2.3.1. Solid ^{31}P NMR characterization

The solid ^{31}P NMR spectra over PDVB-SO_3H and PDVB-SO_3H-SO_2CF_3 were performed as follows: prior to sorption of probe molecules, the sample was placed in a glass tube and then connected to a vacuum line for dehydration. The temperature was gradually increased at a rate of 1 °C/min and the sample was kept at final temperature of 125 °C at a pressure below 10^{-3} Pa over a period of 10 h and then cooled. Detailed procedures involved in introducing the TMPO probe molecule onto the sample can be found elsewhere [56–58]. In brief, a known amount of TMPO adsorbate dissolved in anhydrous CH_2Cl_2 was first added into a vessel containing the dehydrated sample in a N_2 glove box, followed by removal of the CH_2Cl_2 solvent by evacuation at room temperature. To ensure a uniform adsorption of adsorbate probe molecules in the pores/channels of the mesoporous adsorbent, the sealed sample vessel was further subjected to a thermal treatment at 100 °C for 12 h. Prior to NMR measurements, the sealed sample tube was opened and the sample was transferred into a NMR rotor with a Kel-F end cap under a dry nitrogen atmosphere in a glove box.

The solid state NMR experiments were performed on a Varian Infinitypuls-400 spectrometer using a Chemagnetic 5 mm double-resonance probe. A Larmor frequency of 400.13, and 161.98 MHz, and a typical $\pi/2$ pulse length of 6.6, and 3.0 μs were adopted for ^{1}H and ^{31}P resonance, respectively. For the single-pulse ^{31}P MAS NMR experiment, an excitation pulse equivalent to ca. $\pi/4$ and are cycle delay of 15 s were used during spectrum acquisition. The chemical shifts for the ^{31}P resonance were referred to $(NH_4)_2HPO_4$ (0.0 ppm) and the experiments were carried out with a MAS frequency of 8 kHz.

The acid strength over various samples could be also measured by ammonia sorption and temperature programmed desorption (NH_3–TPD) technique. As a typical run, 0.2 g of catalyst (40–60 mesh) was saturated with NH_3 at 30 °C for 45 min. Then, the sample was exposed to the flowing N_2 for removing of the physically adsorbed ammonia on the surface of the sample. Finally desorption of NH_3 was carried out by heating the sample from 30 to 700 °C. Desorption of NH_3 was analyzed by gas chromatography equipped with a TCD detector.

Nitrogen isotherms were measured using a Micromeritics ASAP 2020M system. The samples were outgassed for 10 h at 120 °C before the measurements. The pore-size distribution for mesopores was calculated using Barrett–Joyner–Halenda (BJH) model. FTIR spectra were recorded by using a Bruker 66V FTIR spectrometer. Differential thermal analysis (DTA) and thermogravimetric analysis (TG) were performed on a Perkin-Elmer TGA7 and a DTA-1700 in flowing air, respectively. The heating rate was 10 °C/min. TEM images were performed on a JEM-3010 electron microscope (JEOL, Japan) with an acceleration voltage of 300 kV. Contact angles were tested on DSA10MK2G140, Kruss Company, Germany. XPS spectra were performed on a Thermo ESCALAB 250 with Al Kα radiation at $y = 901$ for the X-ray sources, the binding energies were calibrated using the C_{1s} peak at 284.9 eV.

2.4. Catalytic reactions

2.4.1. Preparation of DNS reagent

As a typical run for preparation of DNS solution, 182 g of potassium sodium tartrate was added into 500 mL of hot deionized water at 50 °C, followed by addition of 6.3 g of 3,5-dinitrosalicylic acid (DNS) and 262 mL of 2 M NaOH, after dissolved, 5 g of phenol and 5 g of sodium sulfite were also introduced into the solution under vigorous stirring, after homogeneous solution was formed, the hot solution was cooled to room temperature and diluted with deionized water to 1000 mL to give the DNS reagent.

2.4.2. Depolymerization of crystalline cellulose

As a typical run, 100 mg of crystalline cellulose of Avicel was dissolved into 2.0 g of $[C_4mim]Cl$ ionic liquid at 100 °C for 1 h under stirring condition until a clear solution was formed. Then, 30 mg of PDVB-$[C_4mim][SO_3CF_3]$ was added, further stirring for 5 min to result in good dispersion of catalyst in reaction mixture, followed by addition of 600 μL of water. At different time intervals, samples were withdrawn, weighed, quenched immediately with cold water, and centrifuged at 14,800 rpm for 5 min for removing of catalysts and unreacted cellulose, giving the reaction mixture, which were collected and stored at 0 °C before DNS assay and HPLC analysis. In the meanwhile, the isolated cellulose was thoroughly washed with water, and recovered by centrifugation. The amount of cellulose isolated was determined by weighing.

2.4.3. Testing total reducing sugar (TRS)

TRS were tested through DNS method [59,60]. As a typical run, a mixture containing of 0.5 mL of DNS regent and 0.5 mL of performed reaction mixture was heated for 5 min at 100 °C, after cooled to room temperature, 4 mL of deionized water was added for diluting the mixture. The color intensity of the mixture was measured in a NanoDrop 2000 UV-spectrophotometer at 540 nm. The concentration of total reducing sugars was calculated based on a standard curve obtained with glucose.

The concentrations of glucose and cellobiose in the reaction mixture were measured by HPLC system, in a Water 717plus autosampler (USA) system, in a Aminex HPX-87H column and with a refraction index detector. The column's temperature was set to 65 °C. The volume of the injection was 10 μL. The eluent consisted of a previously filtered and degasified solution of sulfuric acid 5 mM at a flow of 0.5 (mL/min).

2.4.4. Peckmann reaction

Peckmann reaction of resorcinol with ethyl acetoacetate (PRE) was performed into a three-necked round flask equipped with a condenser and a magnetic stirrer. As a typical run, 0.2 g of catalyst was added into a solution containing of 10 mmol of resorcinol, 10 mmol of ethyl acetoacetate and 10 mL of toluene (solvent) were mixed, then the reaction temperature was increased to 110 °C and lasted for 2 h. The molar ratio of resorcinol/ethyl acetoacetate was 1.0 and the mass ratio of catalyst/reactants was 0.083.

2.4.5. Transesterification

As a typical run of transesterifications of tripalmitin with methanol (TTM): 0.84 g (1.04 mmol) of tripalmitin melted into a three-necked round flask equipped with a condenser and a magnetic stirrer at 65 °C, followed by addition of 3.76 mL of methanol and 0.05 g of catalyst, the reaction was continued for 16 h at 65 °C. In this reaction, the molar ratio of tripalmitin/methanol was nearly 1/90 and the mass ratio of catalyst/tripalmitin was 0.0595.

2.4.6. Hydration

As a typical run for hydration of propylene oxide with water (HPW): 0.1 g of catalyst was added into a solution containing of 50 mmol of propylene oxide and 500 mmol of H_2O at 43 °C, and the reaction was lasted for 6 h. In this reaction, the molar ratio of propylene oxide/water was 0.1 and the mass ratio of catalyst/reactants was 0.0084.

In the reactions of PRE, HPW and TTM, all of the products were analyzed by gas chromatography of Agilent 7890 with a flame ionization detector (FID). The column was HP-INNOWax capillary column (30 m); the initial temperature was 100 °C, ramping rate was 20 °C/min, and final temperature was 280 °C; the temperature of FID detector was 350 °C. In these reactions, dodecane was used as an internal standard.

3. Results and discussion

3.1. Structural characterizations

Fig. 1 shows the N_2 sorption isotherms and pore size distribution of PDVB-SO_3H and PDVB-SO_3H-SO_2CF_3. Clearly, both of the samples exhibit typical type-IV isotherms, giving the steep increase at relative pressure between $0.8 < P/P_0 < 0.95$, confirming the formation of obvious mesoporosity in these samples [61,62]. Additionally, PDVB-SO_3H and PDVB-SO_3H-SO_2CF_3 give the BET surface areas of 314 and 376 m^2/g, respectively (Table 1), much higher than those of SO_4/ZrO_2 (70 m^2/g, Table 1), Amberlyst 15 (40 m^2/g, Table 1) and Nafion NR 50 (0.02 m^2/g, Table 1), lower than those of SBA-15-SO_3H and H form zeolites (820–550 m^2/g, Table 1). Correspondingly, the pore sizes of PDVB-SO_3H and PDVB-SO_3H-SO_2CF_3 are distributed at 22.9 and 29.3 nm (Fig. 1B and Table 1), respectively. It should also be noted that after the introduction of $-SO_2CF_3$ group in PDVB-SO_3H, the BET surface area of PDVB-SO_3H-SO_2CF_3 has certain decreasing because of the introduction of $-SO_2CF_3$ group largely increases

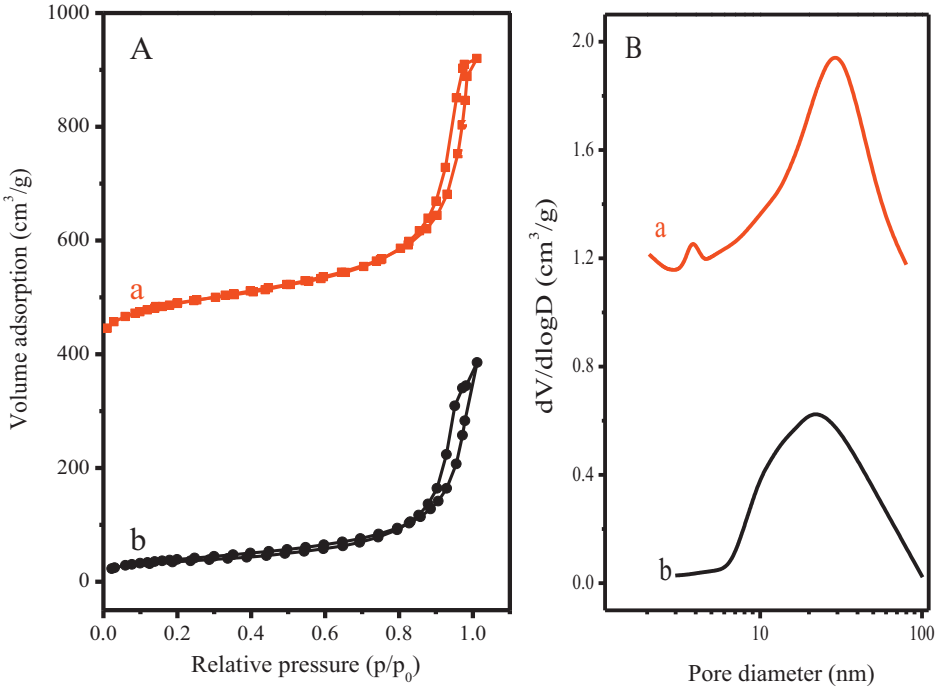

Fig. 1. (A) N_2 sorption isotherms and the pore size distribution of (a) PDVB-SO_3H, and (b) PDVB-SO_3H-SO_2CF_3. The isotherms for (a) was offset by 400 cm^3/g along with vertical axis for clarity, and pore size distribution for (a) was offset by 1.0 cm^3/g along with vertical axis for clarity, respectively.

density of the network and blocks the mesopores of PDVB-SO_3H-SO_2CF_3. Similar result has also been reported previously [8].

Table 1 presents the textural parameters of various samples. Notably, PDVB-SO_3H shows the S content at 3.2 mmol/g. After introduction of electron withdrawing groups of $-SO_2CF_3$ in the sample of PDVB-SO_3H, the corresponding S content was increased up to 5.72 mmol/g, which was much higher than those of Nafion NR50 (0.86 mmol/g, Table 1), SO_4/ZrO_2 (0.72 mmol/g, Table 1), SBA-15-SO_3H (1.36 mmol/g, Table 1), and Amberlyst 15 (4.3 mmol/g, Table 1). The obviously increasing of S content demonstrated that the electron withdrawing group of $-SO_2CF_3$ has been successfully grafted onto the network of PDVB-SO_3H. It should be also noted that the acid capacity is higher than the amount of S for PDVB-SO_3H, which is attributed to partially oxidation of functional group such as C=C bond in PDVB network, further resulting in formation of COOH group and giving increased acid capacity.

Fig. 2 shows the transmission electron microscopy (TEM) images of PDVB-SO_3H and PDVB-SO_3H-SO_2CF_3. Clearly, both PDVB-SO_3H and PDVB-SO_3H-SO_2CF_3 have abundant mesoporosity with the pore sizes ranged from 10 to 50 nm, in good agreement with N_2 sorption isotherms results, the abundant mesoporosity comes from our unique solvothermally synthetic technology [42].

3.2. Wettability characterizations

Fig. 3 shows the contact angle of PDVB-SO_3H-SO_2CF_3 for water and salad oil. Clearly, PDVB-SO_3H-SO_2CF_3 exhibits the contact angle for the water up to 135° (Fig. 2A), indicating its excellent hydrophobicity. On the contrary, for the salad oil, PDVB-SO_3H-SO_2CF_3 gives the contact angle nearly 0° (Fig. 2B), indicating its very good oleophilicity. The superior hydrophobic active site and oleophilic network will be favorable for increasing the exposition degree of active sites for the organic reactants in the processes of various catalytic reactions.

3.3. Active site characterizations

Fig. 4 shows the FT-IR spectra of PDVB, PDVB-SO_3H and PDVB-SO_3H-SO_2CF_3. Compared with PDVB, the peak around 1033–1040 cm^{-1} associated with C—S bond can be clearly found

Table 1
The textural and acidic parameters over various samples.

Samples	S content (mmol/g)[a]	Acid sites (mmol/g)[b]	S_{BET} (m^2/g)	V_P (cm^3/g)	D_P[c] (nm)
PDVB	–	–	700	1.34	23.1
PDVB-SO_3H	3.20	3.50	376	0.90	22.5
PDVB-SO_3H-SO_2CF_3	5.72	3.34	314	0.91	29.3
Amberlyst 15	4.30	4.70	45	0.31	40
Nafion NR50	0.86	0.90	0.02	–	–
SO_4/ZrO_2[d]	0.72	–	70	–	–
SBA-15-SO_3H	1.36	1.26	820	1.40	7.3
H-Beta[e]		1.21	550	0.20	0.67
H-USY[f]		2.06	623	0.26	14.7

[a] Measured by elemental analysis.
[b] Measured by acid–base titration.
[c] Pore size distribution estimated from BJH model.
[d] SO_4/ZrO_2 synthesized as reference of 24.
[e] Si/Al ratio at 12.5.
[f] Si/Al ratio at 7.5.

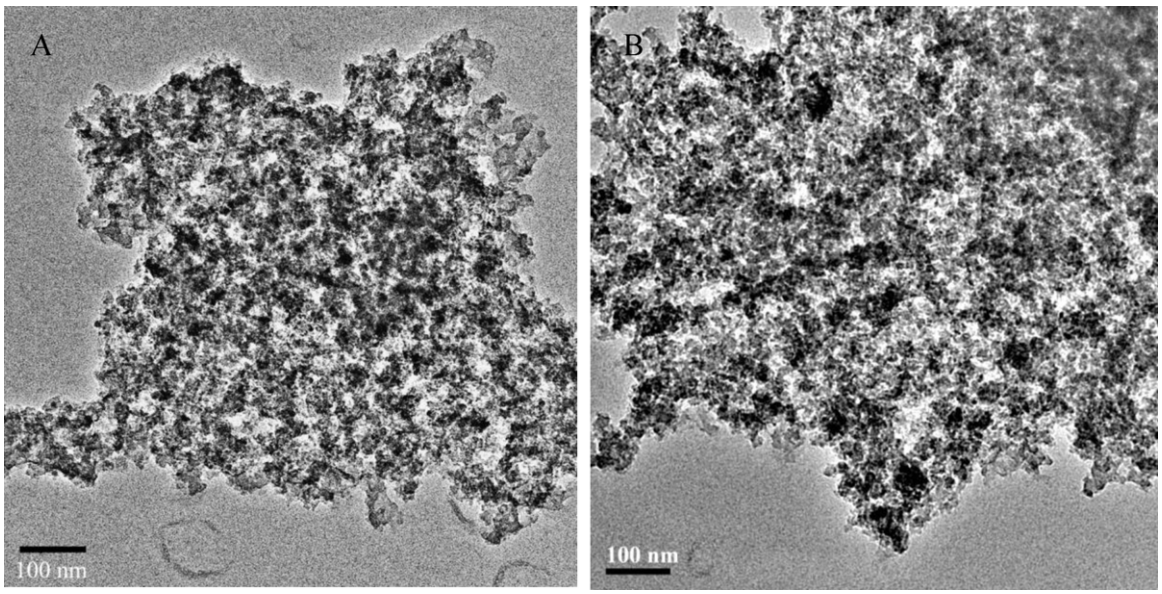

Fig. 2. Transmission electron microscopy images of (A) PDVB-SO_3H and (B) PDVB-SO_3H-SO_2CF_3.

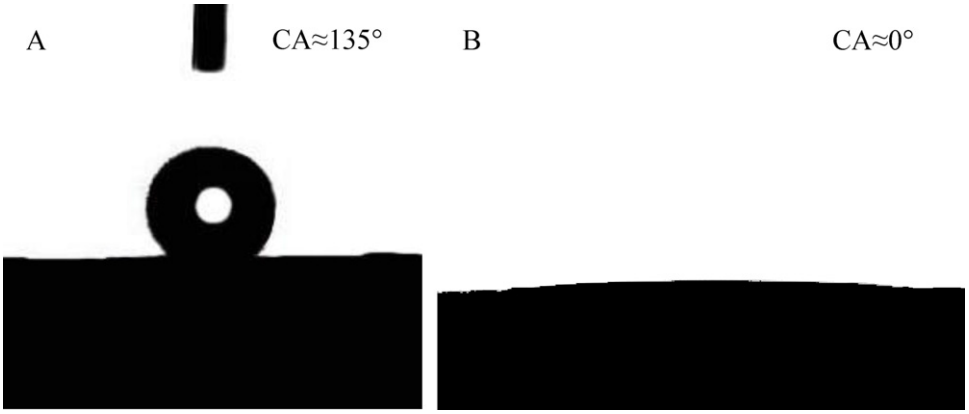

Fig. 3. Contact angles of (A) a water droplet and (B) a salad oil droplet on the surface of PDVB-SO_3H-SO_2CF_3.

in the samples of PDVB-SO_3H and PDVB-SO_3H-SO_2CF_3, suggesting the presence of sulfonic group in these samples [63]. Except for the signal of sulfonic group, a new peak assigned to C—F (1289 cm^{-1}) bond can also be found in PDVB-SO_3H-SO_2CF_3, which confirms the successfully introduction of —SO_2CF_3 group in PDVB-SO_3H [64], in good agreement with element analysis results.

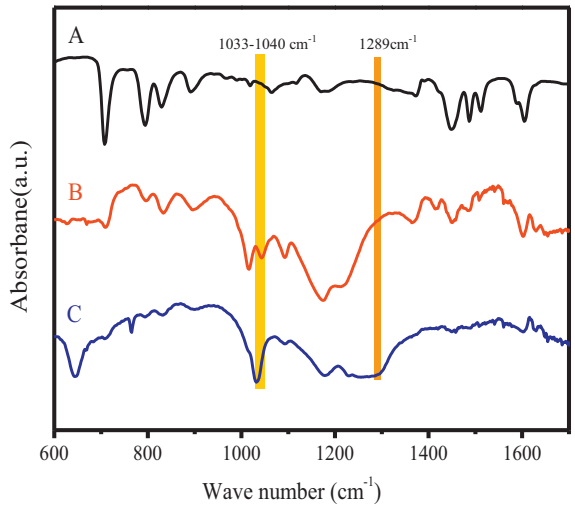

Fig. 4. FT-IR spectra of (A) PDVB, (B) PDVB-SO_3H and (C) PDVB-SO_3H-SO_2CF_3.

Fig. 5 shows the X-ray photoelectron spectroscopy (XPS) measurements of various samples. Clearly, both PDVB-SO_3H and PDVB-SO_3H-SO_2CF_3 show the signals of S, C and O, indicating the presence of sulfonic group in these samples. Except for S, C and O, a new signal at around 690 eV associated with F_{1s} can also be observed in PDVB-SO_3H-SO_2CF_3, confirming successfully grafting of —SO_2CF_3 onto the network of PDVB-SO_3H. Correspondingly, the high resolved XPS spectrum of C_{1s} shows the signals at around 284.7, 286.2 and 291.4 eV associated with C—C, C—S and C—F bond could be found in PDVB-SO_3H-SO_2CF_3, suggesting the successfully introduction of —SO_2CF_3 in PDVB-SO_3H [64]. Interestingly, compared with PDVB-SO_3H, the signal of S_{2p} in PDVB-SO_3H-SO_2CF_3 shifted from 169.1 to 169.5 eV, attributing to the presence of strong electron withdrawing group of —SO_2CF_3 in PDVB-SO_3H-SO_2CF_3, which plays a key factor for increasing the acid strength of PDVB-SO_3H-SO_2CF_3.

3.4. Acid strength

Fig. 6A shows the solid-state ^{31}P MAS NMR of adsorbed TMPO over various samples, which is a unique and practical technique for acidity characterization of solid acid catalysts. Such method has been extensively used to investigate the acidity

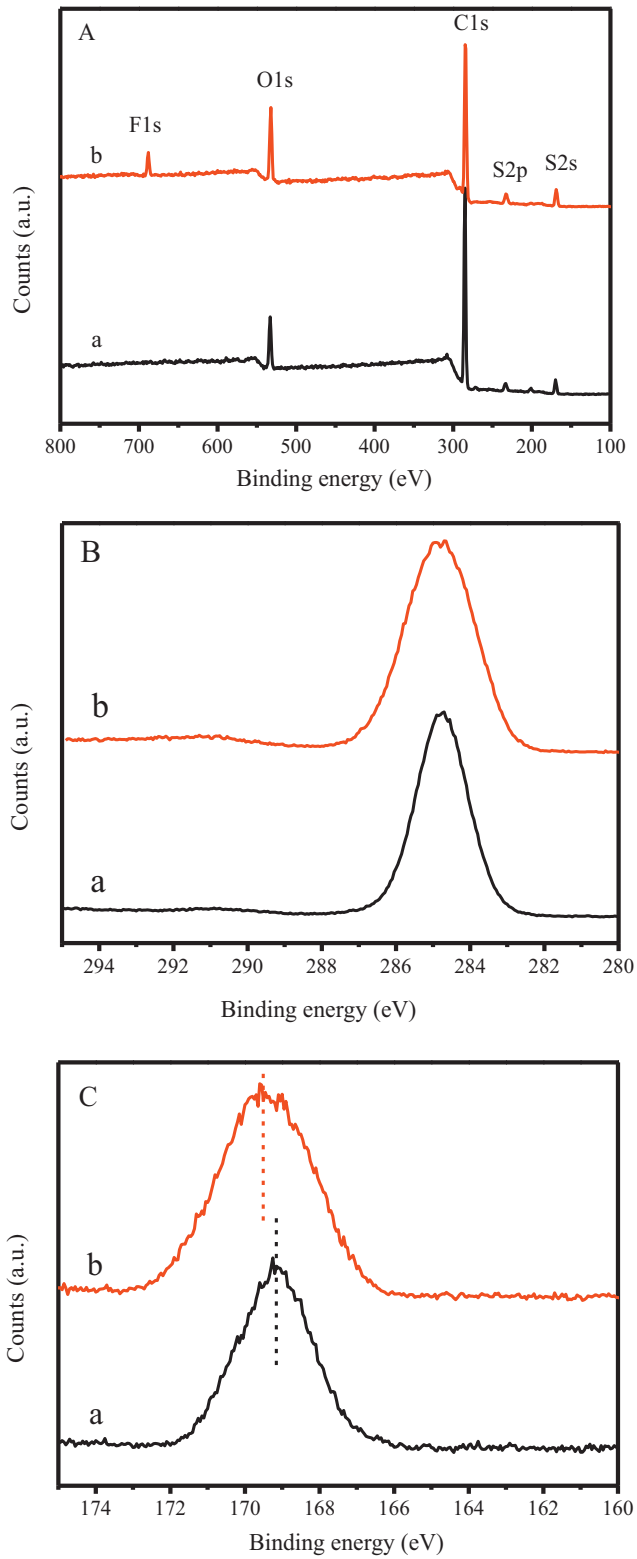

Fig. 5. X-ray photoelectron spectroscopy measurements of (A) survey, (B) C_{1s}, (C) S_{2p} of (a) PDVB-SO_3H and (b) PDVB-SO_3H-SO_2CF_3.

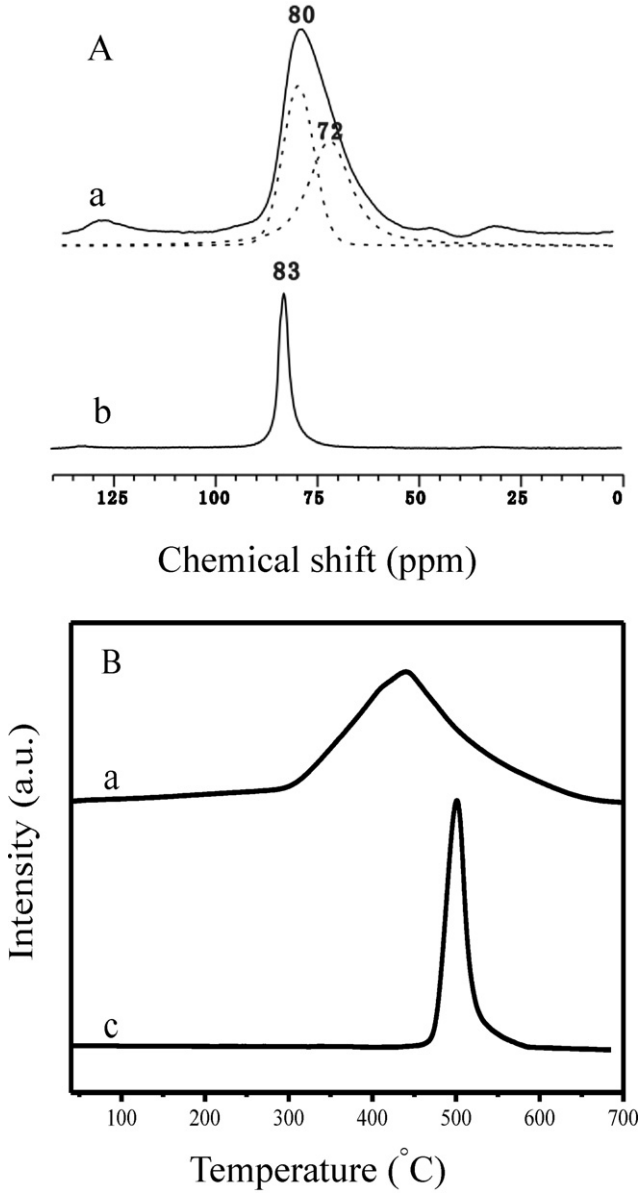

Fig. 6. (A) Solid-state ^{31}P MAS NMR of adsorbed TMPO and (B) NH_3–TPD curves of (a) PDVB-SO_3H and (b) PDVB-SO_3H-SO_2CF_3.

characterization of various solid acids, including zeolites, sulfated mesoporous metal oxides and heteropolyacids [56–59]. As verified by our previous investigations that ^{31}P chemical shift of TMPO can serve as the indicator for the Brønsted acid strength of solid catalysts [56]. Fig. 6A-a displays the ^{31}P MAS NMR spectrum of TMPO adsorbed on PDVB-SO_3H, which shows highly overlapped ^{31}P resonance peaks spanning from ca. 70 to 80 ppm. Further analysis by Gaussian simulation reveals that the spectrum may be deconvoluted into two characteristic resonances with ^{31}P chemical shift of 72 and 80 ppm, each corresponding to a relative concentration of 40 and 60%, respectively. According to the range of the ^{31}P chemical shift, these two ^{31}P resonances above are ascribed unambiguously due to TMPO adsorbed on Brønsted acid sites with various extents of protonation. It is well known that a low-field observed ^{31}P chemical shift value would represent a stronger acidic strength [56–59]. After the treatment by using superacid of HSO_3CF_3, the strong electron withdrawing group of $-SO_2CF_3$ was grafted onto the network of PDVB-SO_3H, resulting in the sample of PDVB-SO_3H-SO_2CF_3. Correspondingly, the Brønsted acidic strength of PDVB-SO_3H-SO_2CF_3 has been significantly enhanced and homogeneously distributed. As shown in Fig. 6A-b, for PDVB-SO_3H-SO_2CF_3, only one uniform ^{31}P peak with chemical shift at 83 ppm can be observed. It is important to note that the Brønsted acidic proton at 83 ppm is much close to the superacid that a theoretical ^{31}P value of 86 ppm was determined as the threshold for superacidity [56–59]. As verified by our

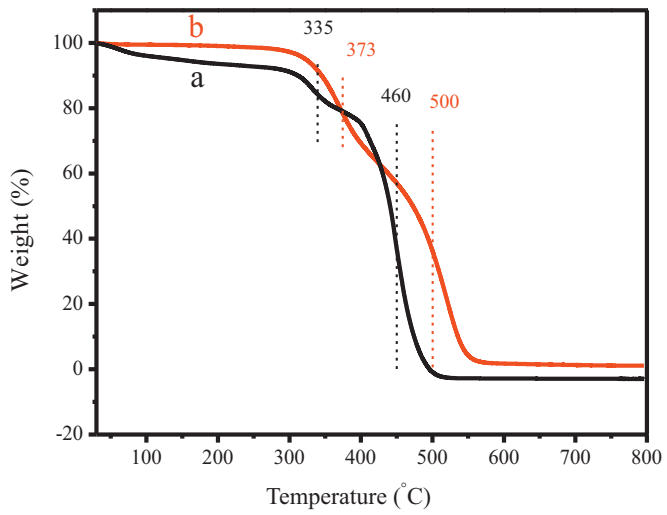

Fig. 7. TG curves of (a) Nafion NR50 and (b) PDVB-SO_3H-SO_2CF_3.

previous investigations based on theoretical calculations, a linear correlation between the ^{31}P chemical shift of TMPO and the proton affinity (PA) values, and hence the strengths of Brønsted acid sites [56]. According to the relationship between the PA and ^{31}P chemical shift ($\delta^{31}P = 182.866 - 0.3902 \times DPE$) [56], the proton affinities are ca. 284, 264 and 256 kcal/mol for the Brønsted acidic sites with TMPO ^{31}P chemical shift at 72, 80 and 83 ppm, respectively. It is clear that the treatment by HSO_3CF_3 can dramatically enhance the acidity and make the acid dispersion more uniform in PDVB-SO_3H, which was favorable for promoting its catalytic activities in various reactions, similar results have not been reported previously.

Fig. 6B shows the NH_3–TPD curves of PDVB-SO_3H and PDVB-SO_3H-SO_2CF_3, which is also an effective method for evaluating the acid strength over various solid acids. Interestingly, PDVB-SO_3H-SO_2CF_3 shows a very sharp NH_3 desorption peak centered at 500 °C, which was much higher and narrower than that of PDVB-SO_3H (440 °C, a very broaden peak), demonstrating its much stronger acid strength and homogeneous acid distribution than that of PDVB-SO_3H, in good agreement with ^{31}P MAS NMR results.

3.5. Thermal stability

Fig. 7 shows the TG curves of PDVB-SO_3H-SO_2CF_3 and Nafion NR50 (one of the most stable acidic resins). Clearly, both of the samples exhibited the weight loss between the temperature 290–430 and 430–575 °C, which are associated with the decomposition of functional groups and the destruction of polymeric network, respectively [8]. Notably, the decomposition temperatures of both acidic group (373 °C) and polymeric network (500 °C) in PDVB-SO_3H-SO_2CF_3 are much higher than that of Nafion NR50 (335 and 460 °C), one of the most stable acidic resins, indicating its excellent thermal stability. The superior stability of PDVB-SO_3H-SO_2CF_3 comes from the presence of electron-withdrawing group and highly cross-linked polymeric network in the sample.

3.6. Catalytic activities and recyclability

Fig. 8 shows the kinetics curves toward depolymerization of crystalline cellulose to sugars catalyzed by PDVB-SO_3H-SO_2CF_3, PDVB-SO_3H and Amberlyst 15, which is one of the most important reactions for production of biofuels, having received extensive attention in recent years [18–22,26,65]. Clearly, PDVB-SO_3H-SO_2CF_3 exhibits much better catalytic activities and selectivity than those of PDVB-SO_3H and Amberlyst 15. For example, the yield of total reducing sugars catalyzed by PDVB-SO_3H-SO_2CF_3 was up to 87.1% for 5 h, much higher than those of PDVB-SO_3H (60.7%) and commercial Amberlyst 15 (50.3%). More interestingly, PDVB-SO_3H-SO_2CF_3 shows very good selectivity for glucose (glucose at 66.2% and cellobiose at 9.1%, Table 2) as compared with those of PDVB-SO_3H (glucose at 34.0% and cellobiose at 11.2%, Table 2) and Amberlyst 15 (glucose at 24.5% and cellobiose at 10.8%, Table 2).

Additionally, PDVB-SO_3H-SO_2CF_3 also shows very good catalytic activities in other type of acid-catalyzed reactions. Table 3 presents the catalytic activities in liquid-catalyzed reactions of HPW, PRE, and TTM over various catalysts. Notably, PDVB-SO_3H-SO_2CF_3 shows much better catalytic activities than those of

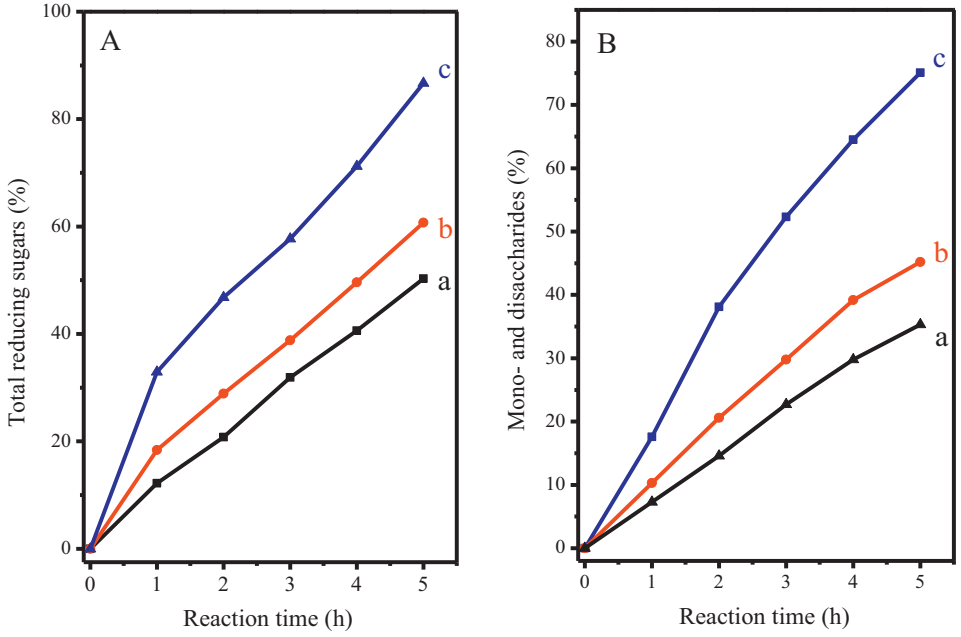

Fig. 8. Catalytic kinetics curves for depolymerization of crystalline cellulose monitored by (A) DNS assay and (B) HPLC catalyzed by (a) Amberlyst 15, (b) PDVB-SO_3H, and (c) PDVB-SO_3H-SO_2CF_3.

Table 2
Yields of sugars and dehydration products in the depolymerization of crystalline cellulose catalyzed by various solid acids.

Run	Samples	Glucose yield (%)[a]	Cellobiose yield (%)[a]	TRS (%)[b]
1	Amberlyst 15	24.5	10.8	50.3
2	PDVB-SO_3H	34.0	11.2	60.7
3	PDVB-SO_3H-SO_2CF_3	66.2	9.1	86.7
4	PDVB-SO_3H-SO_2CF_3[c]	63.4	9.7	84.1

[a] Monitored by HPLC method.
[b] Monitored by DNS assay.
[c] The sample after recycling for five times.

PDVB-SO_3H, Amberlyst 15, SBA-15-SO_3H, acidic zeolites, and solid strong acids of SO_4/ZrO_2 and Nafion NR50. For example, the yield of biodiesel catalyzed by PDVB-SO_3H-SO_2CF_3 was up to 91.4% for 16 h (Table 3, run 2) in biomass transformation toward transesterification to biodiesel, much higher than those of PDVB-SO_3H (73.8%, Table 3, run 1), SO_4/ZrO_2 (53.1%, Table 3, run 4), Nafion NR50 (61.1%, Table 3, run 5), Amberlyst 15 (59.8%, Table 3, run 6) and SBA-15-SO_3H (59.2%, Table 3, run 7). The excellent catalytic activities and good selectivity of PDVB-SO_3H-SO_2CF_3 are mainly attributed to its large BET surface area, good hydrophobic, oleophilic network, ultra strong acid strength and homogeneous acid distributions. On the contrary, although SO_4/ZrO_2 and Nafion NR50 exhibited very strong acid strength, their lower surface areas and hydrophilic frameworks result in relatively low catalytic activities.

It should be note here that after increasing of the contents of typical heterogeneous catalysts such as SBA-15-SO_3H and Nafion NR 50 in the reaction of HPW, which exhibit the same amount of acid sites as that of PDVB-SO_3H-SO_2CF_3, the catalytic activities of SBA-15-SO_3H (69.4%) and Nafion NR 50 (78.6%) were still much lower than that of PDVB-SO_3H-SO_2CF_3 (94.8%). Relatively weak acid strength and partially deactivation of active site in SBA-15-SO_3H resulted from its hydrophilic framework lead to its lower activities; While ultra low BET surface area of Nafion NR50 results in its lower exposition degree of active sites, further resulting in its lower catalytic activity [17].

More importantly, PDVB-SO_3H-SO_2CF_3 shows very good recyclability. For the reaction of crystalline cellulose depolymerization, after recycling for five times, PDVB-SO_3H-SO_2CF_3 gave the total reducing sugars up to 84.1%, very close to that of fresh PDVB-SO_3H-SO_2CF_3 (86.7%, Table 2, run 3); More importantly, the selectivity for glucose and cellobiose catalyzed by recycled PDVB-SO_3H-SO_2CF_3 were 63.4 and 9.7%, respectively, which were very similar as that of fresh PDVB-SO_3H-SO_2CF_3. Additionally, the recyclability of PDVB-SO_3H-SO_2CF_3 in other reaction of PRE was shown in Fig. 9, and obviously decreasing of catalytic activities for PDVB-SO_3H-SO_2CF_3 cannot be found after recycling for 5 times. Moreover, the recycled PDVB-SO_3H-SO_2CF_3 also showed very good catalytic activities in the reactions of TTM and HPW (Table 3, run 3), which were as comparable as that of fresh PDVB-SO_3H-SO_2CF_3 (Table 3, run 3). The superior recyclability of PDVB-SO_3H-SO_2CF_3 comes from its superior thermal stability of both acidic sites and polymer network, which is very important for its widely practical applications.

Collaboration of the unique features of PDVB-SO_3H-SO_2CF_3 including ultra strong acid strength, large BET surface area, superior thermal stability, excellent catalytic activities and good recyclability, PDVB-SO_3H-SO_2CF_3 will be used as novel and efficient solid strong acid catalyst for biofuels production.

Table 3
Catalytic data in Peckmann reaction of resorcinol with ethyl acetoacetate (PRE), transesterification of tripalmitin with methanol (TTM), hydration of propylene oxide with water (HPW) over various catalysts.

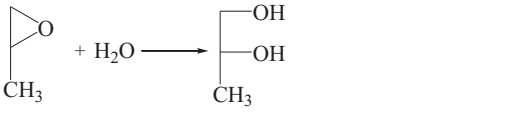

HPW

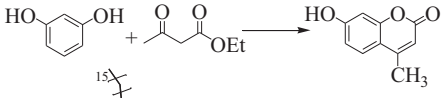

PRE

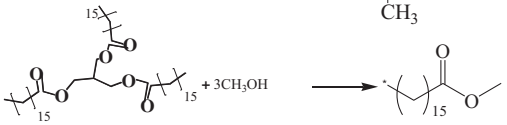

TTM

Run	Catalysts	HPW yield (%)[a]	PRE con. (%)[b]	TTM con. (%)[c]
1	PDVB-SO_3H	78.9	80.9	73.8
2	PDVB-SO_3H-SO_2CF_3	94.8	93.5	91.4
3	PDVB-SO_3H-SO_2CF_3[d]	90.2	91.3	87.8
4	SO_4/ZrO_2	62.1	67.8	53.1
5	Nafion NR50	65.3	78.9	61.1
6	Nafion NR50[e]	78.6		
7	Amberlyst 15	66.7	68.2	59.8
8	SBA-15-SO_3H	55.9	58.9	59.2
9	SBA-15-SO_3H[e]	69.4		
10	H-Beta	31.1	28.7	10.1
11	H-USY	36.7	30.2	14.9

[a] The activities in HPW were evaluated by the yield of 1,2-propylene glycol.
[b] The activities in PRE were evaluated by ethyl acetoacetate conversion.
[c] The activities in TTM were evaluated by the yield of biodiesel.
[d] The samples after recycling for five times.
[e] The same amount of acidic sites as that of PDVB-SO_3H-SO_2CF_3.

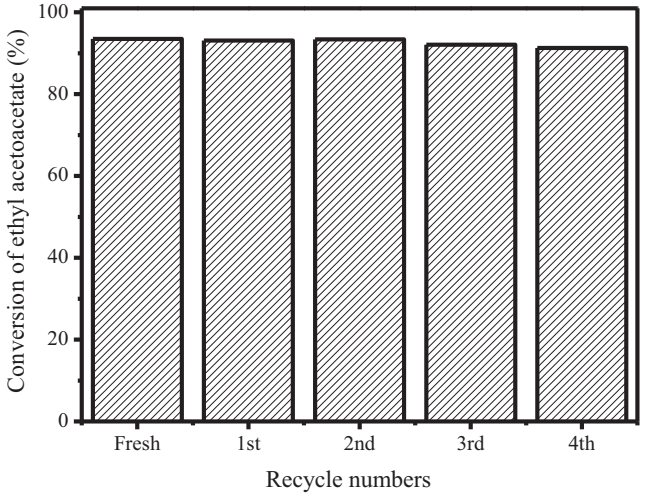

Fig. 9. Recycle numbers over PDVB-SO_3H-SO_2CF_3 in Peckmann reaction of resorcinol with ethyl acetoacetate.

4. Conclusions

Efficient and stable mesoporous polymeric solid strong acid of PDVB-SO_3H-SO_2CF_3 has been successfully prepared through introduction of strong electron withdrawing group of $-SO_2CF_3$ onto the network of PDVB-SO_3H, which showed unique characters including large BET surface area, hydrophobic and oleophilic network, enhanced acid strength and homogeneous acid distribution. The above novel characters of PDVB-SO_3H-SO_2CF_3 result in its excellent catalytic activity and good recyclability in biomass transformations of depolymerization of crystalline cellulose to sugars, and transesterification for production of biodiesel when compared with various conventional solid acids. PDVB-SO_3H-SO_2CF_3 will open new avenues for preparation of porous and stable solid strong acids with abundant mesoporosity, good hydrophobicity and oleophilicity, and excellent catalytic activities and recyclability, which will be potentially important for its wide applications in biomass transformation through green chemical processes in industry.

Acknowledgements

This work was supported by the National Natural Science Foundation of China (21203122 and 21173255), the Foundation of Science and Technology of Shaoxing Bureau (2012B70018) and Postdoctoral Foundation of China (2012M520062).

References

[1] A. Corma, Chemical Reviews 95 (1995) 559.
[2] A. Corma, H. Garcia, Chemical Reviews 103 (2003) 4307.
[3] J.H. Clark, D.J. Macqquarrie, Chemical Society Reviews 25 (1996) 303.
[4] I.V. Kozhevnikov, Chemical Reviews 98 (1998) 171.
[5] R. Sheldon, Chemical Communications 23 (2001) 2399.
[6] M.E. Davis, Nature 417 (2002) 813.
[7] C.W. Jones, K. Tsuji, M.E. Davis, Nature 393 (1998) 52.
[8] F.J. Liu, X.-J. Meng, Y.L. Zhang, L.M. Ren, F. Nawaz, F.-S. Xiao, Journal of Catalysis 271 (2010) 52.
[9] T. Okuhara, Chemical Reviews 102 (2002) 3641.
[10] Y.J. Liu, E. Lotero, J.G. Goodwin Jr., Journal of Catalysis 242 (2006) 278.
[11] Y.J. Xu, W.Q. Gu, D.L. Gin, Journal of the American Chemical Society 126 (2004) 1616.
[12] W. Long, C.W. Jones, ACS Catalysis 1 (2011) 674.
[13] F.J. Liu, T. Willhammar, L. Wang, L.F. Zhu, Q. Sun, X.J. Meng, W. Carrillo-Cabrera, X.D. Zou, F.-S. Xiao, Journal of the American Chemical Society 134 (2012) 4557.
[14] E. Nikolla, Y. Román-Leshkov, M. Moliner, M.E. Davis, ACS Catalysis 1 (2011) 408.
[15] A. Corma, Chemical Reviews 97 (1997) 2373.
[16] J.H. Clark, Accounts of Chemical Research 35 (2002) 791.
[17] F.J. Liu, L. Wang, Q. Sun, L.F. Zhu, X.J. Meng, F.-S. Xiao, Journal of the American Chemical Society 134 (2012) 16948.
[18] Y. Román-Leshkov, C.J. Barrett, Z.Y. Liu, J. Dumesic, Nature 447 (2007) 982.
[19] J.B. Binder, R.T. Raines, Proceedings of the National Academy of Sciences of the United States of America 107 (2010) 4516.
[20] G.W. Huber, J.N. Chheda, C.J. Barrett, J.A. Dumesic, Science 308 (2005) 1446.
[21] E. Andrijanto, E.A. Dawson, D.R. Brown, Applied Catalysis B: Environmental 115–116 (2012) 261.
[22] S. Suganuma, K. Nakajima, M. Kitano, D. Yamaguchi, H. Kato, S. Hayashi, M. Hara, Journal of the American Chemical Society 130 (2008) 12787.
[23] D.H. Zuo, J. Lane, D. Culy, M. Schultz, A. Pullar, M. Waxman, Applied Catalysis B: Environmental 129 (2013) 342.
[24] J.B. Binder, R.T. Raines, Journal of the American Chemical Society 131 (2009) 1979.
[25] L.L. Xu, W. Li, J.L. Hu, X. Yang, Y.H. Guo, Applied Catalysis B: Environmental 90 (2009) 587.
[26] H.L. Cai, C.Z. Li, A.Q. Wang, G.L. Xu, T. Zhang, Applied Catalysis B: Environmental 123–124 (2012) 333.
[27] G.A. Olah, G.K.S. Prakash, J. Sommer, Science 206 (1979) 13.
[28] K. Arata, Applied Catalysis A 146 (1996) 143.
[29] R.J. Gillespie, Accounts of Chemical Research 1 (1968) 202.
[30] R.J. Gillespie, T.E. Peel, Advances in Physical Organic Chemistry 9 (1972) 1.
[31] P. Kalita, B. Sathyaseelan, A. Mano, S.M. Javaid Zaidi, M.A. Chari, A. Vinu, Chemistry: A European Journal 16 (2010) 2843.
[32] X. Song, A. Sayari, Catalysis Reviews: Science and Engineering 38 (1996) 329.
[33] G.D. Yadav, J.J. Nair, Microporous and Mesoporous Materials 33 (1999) 1.
[34] K. Arata, M. Hino, Materials Chemistry and Physics 26 (1990) 213.
[35] Y.Y. Sun, L. Zhu, H.J. Lu, R.W. Wang, S. Lin, D.Z. Jiang, F.-S. Xiao, Applied Catalysis A 237 (2002) 21.
[36] J. Macht, R.T. Carr, E. Iglesia, Journal of Catalysis 264 (2009) 54.
[37] Q.H. Yang, J. Liu, J. Yang, M.P. Kapoor, S. Inagaki, C. Li, Journal of Catalysis 228 (2004) 265.
[38] K. Arata, Applied Catalysis A 146 (1996) 3.
[39] Y.C. Du, S. Liu, Y.L. Zhan, C.Y. Yin, Y. Di, F.-S. Xiao, Catalysis Letters 108 (2006) 155.
[40] K. Okuyama, X. Chen, K. Takata, D. Odawara, T. Suzuki, S.I. Nakata, T. Okuhara, Applied Catalysis A 190 (2000) 253.
[41] M. Kimura, T. Nakato, T. Okuhara, Applied Catalysis A 165 (1997) 227.
[42] F.J. Liu, W.P. Kong, C.Z. Qi, L.F. Zhu, F.-S. Xiao, ACS Catalysis 2 (2012) 565.
[43] P. Barbaro, F. Liguori, Chemical Reviews 109 (2009) 515.
[44] A. Heidekum, M.A. Harmer, W.F. Hoelderich, Journal of Catalysis 188 (1999) 230.
[45] M.A. Harmer, Q. Sun, Applied Catalysis A 221 (2001) 45.
[46] E. Lam, E. Majid, A.C.W. Leung, J.H. Chong, K.A. Mahmoud, J.H.T. Luong, ChemSusChem 4 (2011) 535.
[47] F. Martínez, G. Morales, A. Martín, R. van Grieken, Applied Catalysis A 347 (2008) 169.
[48] M.C. Laufer, H. Hausmann, W.F. Hölderich, Journal of Catalysis 218 (2003) 315.
[49] R. Xing, N. Liu, Y.M. Liu, H.H. Wu, Y.W. Jiang, L. Chen, M.Y. He, P. Wu, Advanced Functional Materials 17 (2007) 2455.
[50] G. Morales, G. Athens, B.F. Chmelka, R. van Grieken, J.A. Melero, Journal of Catalysis 254 (2008) 205.
[51] M.A. Harmer, Q. Sun, W.E. Farneth, Journal of the American Chemical Society 118 (1996) 7708.
[52] M.A. Harmer, Q. Sun, A.J. Vega, W.E. Farneth, A. Heidekum, W.F. Hoelderich, Green Chemistry 6 (2000) 7.
[53] F.J. Liu, S.F. Zuo, W.P. Kong, C.Z. Qi, Green Chemistry 14 (2012) 1342.
[54] I. Jiménez-Morales, J. Santamaría-González, P. Maireles-Torres, A. Jiménez-López, Applied Catalysis B: Environmental 123–124 (2012) 316.
[55] D. Margolese, J.A. Melero, S.C. Christiansen, B.F. Chmelka, G.D. Stucky, Chemistry of Materials 12 (2000) 2448.
[56] A. Zheng, H. Zhang, X. Lu, S.B. Liu, F. Deng, Journal of Physical Chemistry B 112 (2008) 4496.
[57] A. Zheng, S. Huang, S.B. Liu, F. Deng, Physical Chemistry Chemical Physics 13 (2011) 14889.
[58] N. Feng, A. Zheng, S.J. Huang, H. Zhang, N. Yu, C.Y. Yang, S.B. Liu, F. Deng, Journal of Physical Chemistry C 114 (2010) 15464.
[59] C. Tagusagawa, A. Takagaki, A. Iguchi, K. Takanabe, J.N. Kondo, K. Ebitani, S. Hayashi, T. Tatsumi, K. Domen, Angewandte Chemie International Edition 49 (2010) 1128.
[60] R. Rinaldi, R. Palkovits, F. Schüth, Angewandte Chemie International Edition 47 (2008) 8047.
[61] D.Y. Zhao, Q.S. Huo, J.L. Feng, B.F. Chmelka, G.D. Stucky, Journal of the American Chemical Society 120 (1998) 6024.
[62] D.Y. Zhao, J.L. Feng, Q.S. Huo, N. Melosh, G.H. Fredrickson, B.F. Chmelka, G.D. Stucky, Science 279 (1998) 548.
[63] J. Scaranto, A.P. Charmet, S. Giorgianni, Journal of Physical Chemistry C 112 (2008) 9443.
[64] C. Koibeck, M. Killian, F. Maier, N. Paape, P. Wasserscheid, H.-P. Steinrück, Langmuir 24 (2008) 9500.
[65] J. Tollefson, Nature 451 (2008) 880.